

# $\omega N$ final state interactions and $\omega$ -meson production from heavy-ion collisions

G.I. Lykasov<sup>1</sup>, W. Cassing<sup>2</sup>, A. Sibirtsev<sup>2</sup>, M.V. Rzjanin<sup>1</sup>

<sup>1</sup> *Joint Institute for Nuclear Research,  
141980 Dubna, Moscow Region, Russia*

<sup>2</sup> *Institut für Theoretische Physik  
Heinrich-Buff-Ring 16, D-35392 Giessen, Germany*

We calculate the elastic and inelastic  $\omega N \rightarrow \omega N$ ,  $\rightarrow \pi N$ ,  $\rightarrow \rho N$ ,  $\rightarrow \rho \pi N$ ,  $\rightarrow \pi \pi N$ ,  $\rightarrow \sigma N$  reactions within a boson exchange approximation where the  $\omega \rho \pi$  coupling constant and form factor are fixed by the reaction  $\pi N \rightarrow \omega N$  in comparison to the experimental data. We find rather large  $\omega N$  cross sections at low relative momenta of the  $\omega$ -meson which leads to a substantial broadening of the  $\omega$ -meson width in nuclear matter. The implications of the  $\omega N$  final state interactions are studied for  $\omega$  production in  $^{12}C + ^{12}C$ ,  $^{40}Ca + ^{40}Ca$  and  $^{58}Ni + ^{58}Ni$  reactions at about  $2 \cdot A$  GeV within the HSD transport approach; the drastic changes of the transverse mass spectra relative to a general  $m_T$ -scaling (for  $\pi^0$  and  $\eta$  mesons) might be controlled experimentally by the TAPS Collaboration.

PACS: 25.75.-q; 25.80.-e

## I. INTRODUCTION

The properties of hadrons in a dense and hot nuclear medium are of fundamental interest with respect to the question of chiral symmetry restoration in such an environment, where a new phase of strongly interacting matter might be encountered [1–4]. The properties of vector mesons here are of particular interest since these can be studied experimentally via their decay to dileptons. Whereas the  $\rho$ -meson spectral function in the medium has been discussed to a large extent [5–8] the properties of the  $\omega$ -meson in dense matter especially at finite relative momentum are achieving increasing interest [9–16]. As in case of the  $\rho$ -meson the  $\omega$ -meson properties at low baryon density are dominantly determined by the interactions with nucleons; real and imaginary parts of the scattering amplitude then are determined by dispersion relations. It is thus of fundamental interest to obtain some information about the  $\omega N$  scattering cross sections which except for the channel  $\pi N \rightarrow \omega N$  are not accessible by experiment.

In this work we address the latter question in a boson-exchange approach and study the implications from the  $\omega N$  final state interactions for  $\omega$  production in nucleus-nucleus reactions around  $2 \cdot A$  GeV in the context of present experiments by the TAPS Collaboration. In Section 2 we will calculate the various elementary  $\omega N$  channels within a boson-exchange model and discuss the uncertainties due to coupling constants and form factors. The transport calculations within the HSD approach [17] for  $\omega$ -meson production in nucleus-nucleus reactions will be presented in Section 3. A summary and discussion of open questions concludes this work in Section 4.

## II. $\omega N$ CROSS SECTIONS

We start by recalling some general features of the  $\omega N$  cross section. Since the  $\omega$ -meson mass is about 5.5 times larger than the pion mass, at low  $\omega$ -meson momenta the exothermic reactions like  $\omega N \rightarrow \pi N$ ,  $\omega N \rightarrow 2\pi N$ ,  $\omega N \rightarrow 3\pi N$  and other channels with a production up to 5  $\pi$ -mesons should be dominant and the corresponding inelastic cross section behave as  $\sigma_{inel} \approx 1/p_\omega$ , where  $p_\omega$  denotes the laboratory momentum. When the total mass of the final particle becomes equal to the total mass of the incident ones, e.g. in the  $\omega N \rightarrow \rho N$  or  $\omega N \rightarrow \omega N$  reaction, the relevant cross section should approach some constant at low  $p_\omega$ . On the other hand the endothermic inelastic reactions, where the total mass of the produced particles is larger than the initial mass, have a threshold behaviour and are more important at high energies.

The amount of the available  $\omega N$  reaction channels, especially in the inelastic sector, is quite large. Thus one needs a reliable model for the  $\omega$ -nucleon interaction at energies up to few GeV. The complexity of the problem has been addressed in the recent studies from Klingl, Kaiser and Weise [12,13] and Friman [15,16], where some of the  $\omega N$  reaction channels were calculated. However, as pointed out in Refs. [15,16] the calculated results are very sensitive to the parameters of the model, i.e. coupling constants, form factors, etc.

As a first step for a simplification we adopt the  $\omega \rho \pi$  dominance model proposed by Gell-Mann, Sharp and Wagner [18] as well as the  $\sigma$  exchange approximation. In practice we restrict to the diagrams shown in Fig 1 which contain the  $\omega \rho \pi$ -vertex and the  $\omega \sigma \omega$ -vertex. In this way we expect to obtain lower bounds especially on the total inelastic scattering cross section.

One way to construct the  $\omega \rho \pi$  Lagrangian is due to the current-field identities of Kroll, Lee and Zumino [19], where the isoscalar and isovector parts of the electromagnetic current – with the  $\omega$ - and  $\rho$ -meson currents, respectively – can be identified. Starting with the Lagrangian for the vector-meson photoproduction on the nucleon one can construct the corresponding Lagrangian for the vector meson-nucleon interaction as in Ref. [20]. The photoproduction of  $\rho$  and  $\omega$ -mesons on the nucleon close to threshold ( $E_\gamma \leq 2$  GeV) has been analyzed by Friman and Soyeur [20] also within the framework of the one-boson exchange (OBE) model. In this sense the OBE model can be applied to elastic and inelastic  $\omega N$  interactions. Furthermore, the relevant coupling constant  $g_{\omega \rho \pi}$  as well as the corresponding form factor can be taken from the earlier analysis in Ref. [20]. In the present work we additionally consider  $\omega \sigma \omega$ -vertices and discuss the uncertainties related to the coupling constants and form factors at the vertices. The lat-

ter uncertainties are reduced to a large extent by the analysis of experimental data on the  $\pi N \rightarrow \omega N$  (or inverse  $\omega N \rightarrow \pi N$ ) reaction.

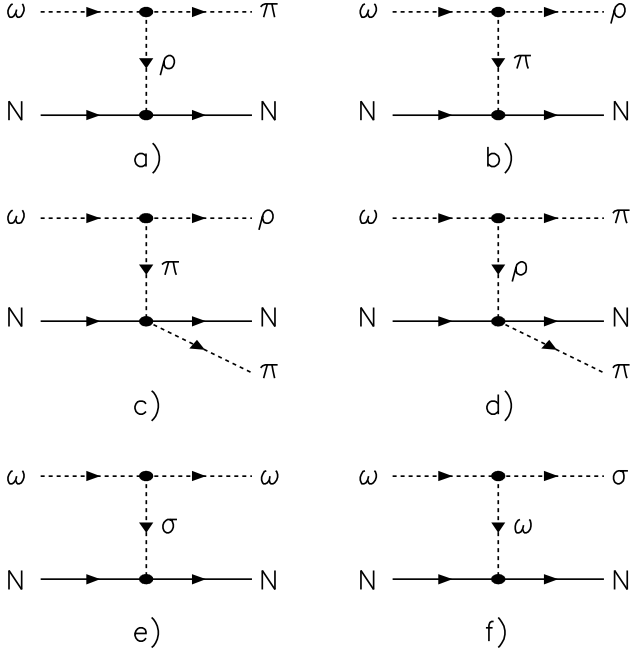


FIG. 1. The diagrams for the  $\omega N$  reaction channels evaluated in the text.

### A. The channel $\omega N \rightarrow \pi N$

The  $\omega N \rightarrow \pi N$  cross section can be controlled by the experimental data on the inverse reaction via detailed balance. The OBE diagram within our approach for the  $\pi N \rightarrow \omega N$  reaction is described by the  $\rho$ -meson exchange as shown in Fig. 1a). For our present study we adopt an effective Lagrangian for the  $\omega\rho\pi$  interaction as

$$\mathcal{L}_{\omega\rho\pi} = \frac{g_{\omega\rho\pi}}{m_\omega} \epsilon_{\alpha\beta\gamma\delta} \partial^\alpha \rho^\beta \partial^\gamma \omega^\delta \pi, \quad (1)$$

where the coupling constant  $g_{\omega\rho\pi} = 10.88$  is taken from Ref. [21],  $\epsilon_{\alpha\beta\gamma\delta}$  denotes the antisymmetric tensor while  $\rho$ ,  $\omega$  and  $\pi$  are the corresponding meson fields. The  $\rho NN$  Lagrangian is taken as

$$\mathcal{L}_{\rho NN} = -g_{\rho NN} \left( \bar{N} \gamma^\mu \tau N \cdot \rho_\mu + \frac{\kappa}{2m_N} \bar{N} \sigma^{\mu\nu} \tau N \cdot \partial_\mu \rho_\nu \right), \quad (2)$$

where  $N$  stands for the nucleon field,  $\tau$  for the Pauli matrices,  $g_{\rho NN} = 3.24$  according to Ref. [22], while the tensor coupling constant is given by the ratio  $\kappa = f_{\rho NN}/g_{\rho NN} = 6.1$ .

The  $\pi N \rightarrow \omega N$  differential cross section then is given by

$$\frac{d\sigma}{dt} = \frac{g_{\omega\rho\pi}^2}{m_\omega^2} \frac{(t + m_\omega^2 - m_\pi^2)^2 - 4m_\omega^2 t}{64\pi \lambda(s, m_\pi^2, m_N^2)}$$

$$\times \frac{F_{\omega\rho\pi}^2(t) F_{\rho NN}^2(t)}{(t - m_\rho^2)^2} \left[ g_{\rho NN}^2 (2t + 4m_N^2) \right. \\ \left. + f_{\rho NN}^2 \left( 3t + 5m_N^2 + \frac{t^2}{4m_N^2} \right) + 8t g_{\rho NN} f_{\rho NN} \right], \quad (3)$$

where  $s$  is the squared invariant collision energy,  $t$  the 4-momentum transferred from the initial to the final nucleon and

$$\lambda(x, y, z) = (x - y - z)^2 - 4yz. \quad (4)$$

For both vertices in the diagram Fig. 1a) we use the form factor

$$F(t) = \frac{\Lambda^2 - m_\rho^2}{\Lambda^2 - t}, \quad (5)$$

which fulfills the on-shell condition  $F(t=m_\rho^2)=1$ . The value for the cut-off parameter in the  $\rho NN$  vertex,  $\Lambda_2=1.4$  GeV, is taken from Ref. [22].

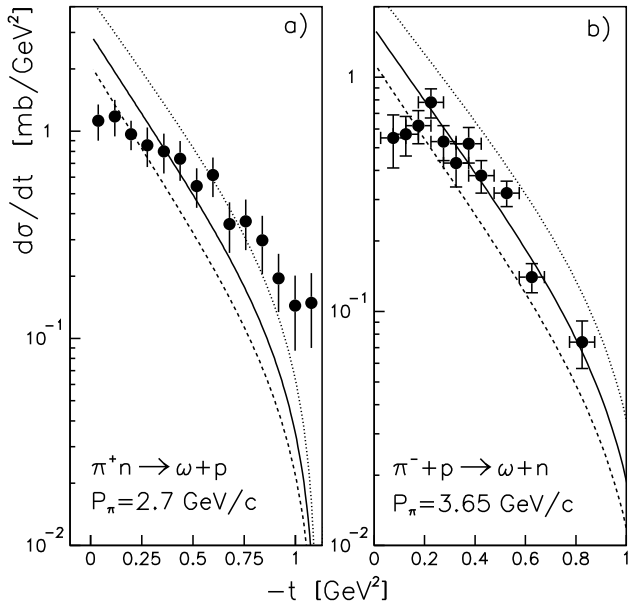


FIG. 2. The  $\pi^+ n \rightarrow \omega p$  (a) and  $\pi^- p \rightarrow \omega n$  (b) differential cross sections as a function of the transferred 4-momentum in comparison to the data taken from Refs. [23,24]. The lines show our calculations for the cut-off parameters  $\Lambda_1 = 1.07$  GeV (solid),  $\Lambda_1 = 1.2$  GeV (dashed) and  $\Lambda_1 = 1.0$  GeV (dotted).

To fix the cut-off in the  $\omega\rho\pi$ -vertex we fit the experimental data on the  $\pi N \rightarrow \omega N$  reaction. Fig. 2a) shows the  $\pi^+ n \rightarrow \omega p$  differential cross section [23] at a pion momentum  $p_\pi = 2.7$  GeV/c together with our calculations for different  $\Lambda_1$  parameters; Fig. 2b) shows the comparison to the  $\pi^- p \rightarrow \omega n$  data [24] at  $p_\pi = 3.65$  GeV/c. A good description is obtained with the cut-off  $\Lambda_1 = 1070$  MeV. However, we observe a systematical discrepancy between our calculations within the  $\rho$ -meson exchange model and the experimental data at low transverse momenta which might be due to an interference with another diagram taken not into account.

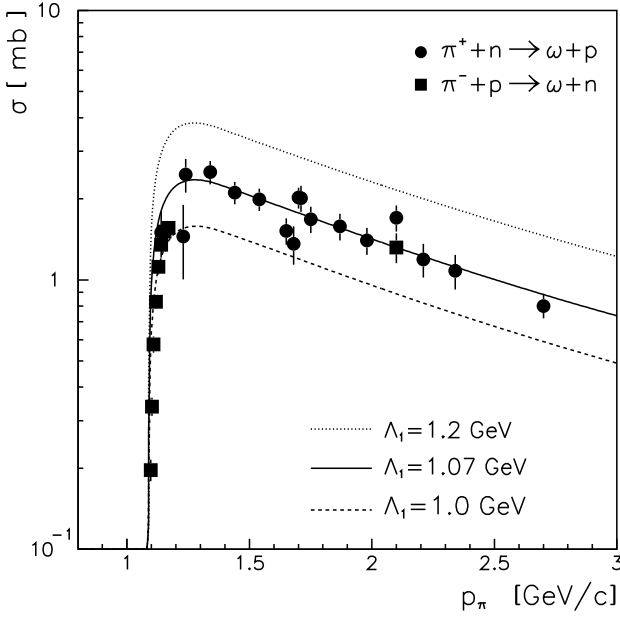


FIG. 3. The  $\pi^+ n \rightarrow \omega p$  and  $\pi^- p \rightarrow \omega n$  total cross sections as function of the pion momentum in comparison to the data from Ref. [25]. The lines show our calculations for the cut-off parameters  $\Lambda_1 = 1.07$  GeV (solid),  $\Lambda_1 = 1.0$  GeV (dashed) and  $\Lambda_1 = 1.2$  GeV (dotted).

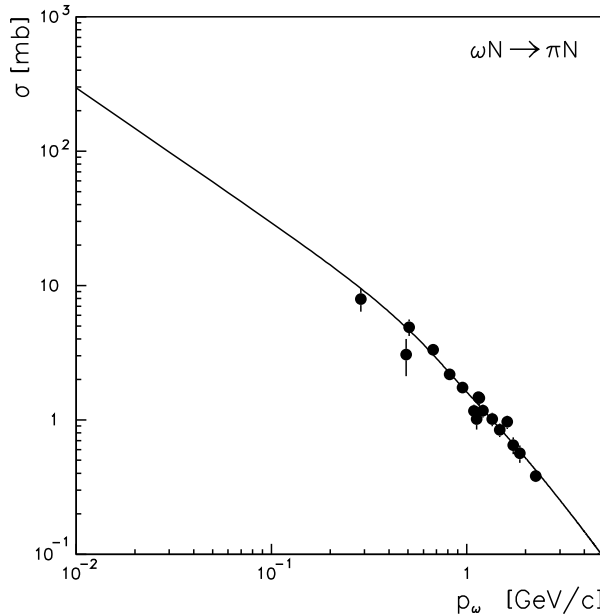


FIG. 4. The cross section for the  $\omega N \rightarrow \pi N$  reaction as a function of the laboratory  $\omega$ -momentum. The solid line is our calculation while the full circles show the  $\omega p \rightarrow \pi^+ n$  experimental data obtained by detailed balance.

Furthermore, Fig. 3 shows the total experimental  $\pi^+ n \rightarrow \omega p$

and  $\pi^- p \rightarrow \omega n$  cross sections [25] as a function of the pion momentum in comparison to our calculations. Again the data are reasonably reproduced with  $\Lambda_1 = 1070$  MeV, which we now fix for the following analysis.

The calculated cross section for the inverse reaction  $\omega N \rightarrow \pi N$  is shown in Fig. 4 for  $\Lambda_1 = 1070$  MeV as function of the  $\omega$ -momentum in the laboratory in comparison to the experimental data obtained by detailed balance.

### B. The channel $\omega N \rightarrow \rho N$

The  $\omega N \rightarrow \rho N$  cross section can be calculated in the one-pion exchange model using the diagram in Fig. 1b). The Lagrangian for the  $\omega\rho\pi$  interaction is given by Eq. (1), while the  $\pi NN$  Lagrangian taken as

$$\mathcal{L}_{\pi NN} = -ig_{\pi NN} \bar{N} \gamma_5 \tau \cdot \pi \quad (6)$$

with the coupling constant  $g_{\pi NN} = 13.59$  [26].

The  $\omega N \rightarrow \rho N$  differential cross section then is given by

$$\frac{d\sigma}{dt} = -g_{\pi NN}^2 t \frac{g_{\omega\rho\pi}^2}{m_\omega^2} \frac{(t - m_\omega^2 - m_\rho^2)^2 - 4m_\omega^2 m_\rho^2}{96\pi} \times \frac{F_{\omega\rho\pi}^2(t) F_{\pi NN}^2(t)}{(t - m_\pi^2)^2}, \quad (7)$$

where the coupling constant and the form factor for the  $\omega\rho\pi$ -vertex is fixed by the  $\pi N \rightarrow \omega N$  calculations. The  $\pi NN$  form factor was taken as in Eq. (5) with the cut-off parameter  $\Lambda = 1.05$  GeV in line with Ref. [27].

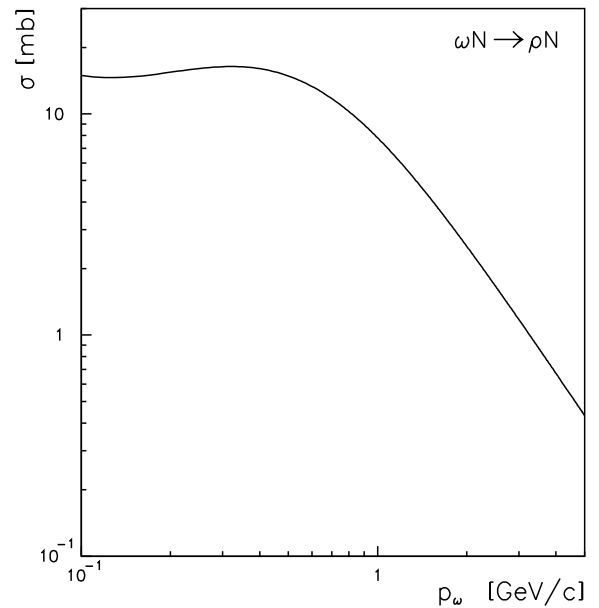


FIG. 5. The cross sections for the  $\omega N \rightarrow \rho N$  reaction.

The resulting  $\omega N \rightarrow \rho N$  cross section is shown by the solid line in Fig. 5 as a function of  $\omega$ -meson laboratory momentum; as mentioned before the cross section is practically constant

at low momentum ( $\approx 15$  mb) and levels off at higher momenta due to the form factors involved. However, above momenta of about 200 MeV/c it is already larger than for the  $\pi N$  final channel.

### C. The channel $\omega N \rightarrow \rho\pi N$

The relevant diagram for the reaction  $\omega N \rightarrow \rho\pi N$  is shown in Fig. 1c) and the corresponding total cross section can be calculated by using the Berestetsky-Pomeranchuk approach [28] as

$$\sigma = \frac{1}{48\pi^2 \lambda(s, m_N^2, m_\omega^2)} \int_{(m_N + m_\pi)^2}^{(\sqrt{s} - m_\rho)^2} ds_1 \lambda^{1/2}(s_1, m_\pi^2, m_N^2) \times \sigma_{\pi N}(s_1) \int_{t_-}^{t_+} dt \frac{g_{\omega\rho\pi}^2 F_{\omega\rho\pi}^2}{m_\omega^2 (t - m_\pi^2)^2} \times \left[ (t - m_\omega^2 - m_\rho^2)^2 - 4m_\omega^2 m_\rho^2 \right], \quad (8)$$

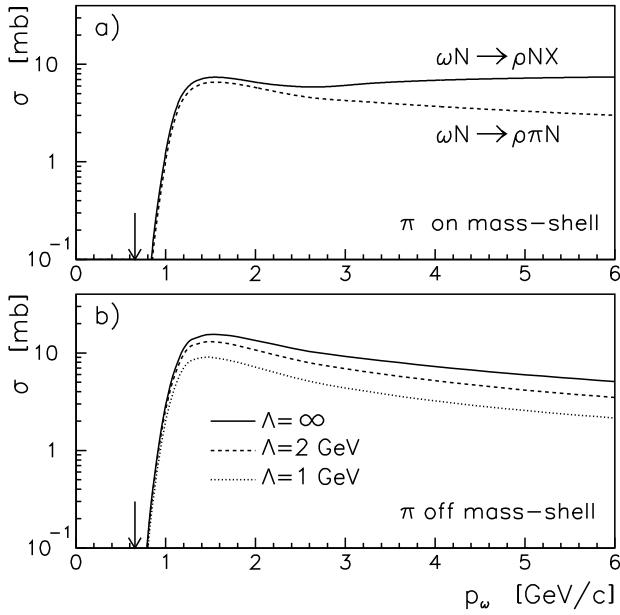


FIG. 6. a): The exclusive  $\omega N \rightarrow \rho\pi N$  (dashed line) and inclusive  $\omega N \rightarrow \rho N X$  cross sections calculated with the one-pion exchange model and within the on mass-shell approximation. The arrow indicates the threshold for the exclusive reaction. b): The exclusive  $\omega N \rightarrow \rho\pi N$  cross section calculated within the off mass-shell approach for different cut-off parameters  $\Lambda$  in the  $\pi N \rightarrow \pi N$  vertex.

In Eq.(8)  $s_1$  is the squared invariant mass of the final  $\pi N$  system,  $\sigma_{\pi N}$  is the  $\pi N \rightarrow \pi N$  elastic cross section taken from Ref. [25] and

$$t^\pm = m_\omega^2 + m_\pi^2 - \frac{1}{2s} \left[ (s + m_\omega^2 - m_N^2) \times (s + m_\rho^2 - s_1) \mp \lambda^{1/2}(s, m_\omega^2, m_N^2) \lambda^{1/2}(s, m_\rho^2, s_1) \right]. \quad (9)$$

The resulting  $\omega N \rightarrow \rho\pi N$  cross section is shown in Fig. 6a) by the dashed line while the arrow indicates the corresponding reaction threshold. Now replacing the elastic  $\pi N \rightarrow \pi N$  cross section in Eq. (8) by the total cross section  $\pi N \rightarrow NX$  we obtain an estimate for the inclusive  $\omega N \rightarrow \rho N X$  cross section, which is shown in terms of the solid line in Fig. 6a). This channel provides an inelastic  $\omega N$  cross section of about  $\simeq 7$  mb at higher momenta.

In Fig. 6a) we have adopted the on-shell approximation [28]. The off-shell correction to the  $\pi N$  amplitude can be estimated e.g. as proposed by Ferrari and Selleri [29], i.e. replacing  $t \rightarrow m_\pi^2$  in the  $\lambda$ -function of Eq. 8 and introducing the form factor

$$F(t) = \frac{\Lambda^2 - m_\pi^2}{\Lambda^2 - t} \quad (10)$$

at the  $\pi N \rightarrow \pi N$  vertex.

The solid line in Fig. 6b) indicates the corresponding calculation when neglecting the form factor at the  $\pi N \rightarrow \pi N$  vertex, the dashed line shows the calculations with the cut-off parameter  $\Lambda = 2$  GeV, while the dotted line corresponds to  $\Lambda = 1$  GeV. Note, that the uncertainty due to the cut-off parameter is quite large when varying  $\Lambda$  from 1 GeV to  $\infty$ . However, the comparison between the dashed line in Fig. 6a) and the dotted line in Fig. 6b) indicates that the results obtained for  $\Lambda = 1$  GeV (in line with Ref. [30]) are in a reasonable agreement with the on mass-shell calculations. Thus in the following we will adopt the on mass-shell approximation.

### D. The channel $\omega N \rightarrow 2\pi N$

The  $\omega N \rightarrow 2\pi N$  cross section can be calculated in the  $\rho$ -meson exchange model as shown by the diagram in Fig. 1d). By taking into account the on-shell  $\rho N \rightarrow \pi N$  amplitude the total cross section is given as

$$\sigma = \frac{1}{32\pi^2 \lambda(s, m_N^2, m_\omega^2)} \int_{(m_N + m_\pi)^2}^{(\sqrt{s} - m_\pi)^2} ds_1 \lambda^{1/2}(s_1, m_\rho^2, m_N^2) \times \sigma_{\rho N \rightarrow \pi N}(s_1) \int_{t_-}^{t_+} dt \frac{g_{\omega\rho\pi}^2 F_{\omega\rho\pi}^2}{m_\omega^2 (t - m_\rho^2)^2} \times \left[ (t + m_\omega^2 - m_\pi^2)^2 - 4tm_\omega^2 \right], \quad (11)$$

where

$$t^\pm = m_\omega^2 + m_\pi^2 - \frac{1}{2s} \left[ (s + m_\omega^2 - m_N^2) \times (s + m_\rho^2 - s_1) \mp \lambda^{1/2}(s, m_\omega^2, m_N^2) \lambda^{1/2}(s, m_\rho^2, s_1) \right]. \quad (12)$$

In Eq. (11) the  $\rho N \rightarrow \pi N$  cross section was taken as in Ref. [31],

$$\sigma_{\rho N \rightarrow \pi N}(s_1) = \frac{\pi^2}{3} \frac{a}{\lambda^{1/2}(s_1, m_\rho^2, m_N^2)} \times \frac{\Gamma^2}{(\sqrt{s_1} - M)^2 + \Gamma^2/4}, \quad (13)$$

with the parameters  $a=413 \text{ } \mu\text{b}/\text{GeV}^2$ ,  $M=1.809 \text{ GeV}$  and  $\Gamma=0.99 \text{ GeV}$ . Note, that the function  $\lambda^{1/2}$  in Eq. (11) is cancelled by Eq. (13). The cross section  $\omega N \rightarrow 2\pi N$  calculated with Eq. (11) is shown in Fig. 7 and approaches 10 mb for low omega momenta, but drops off fast with higher momentum.

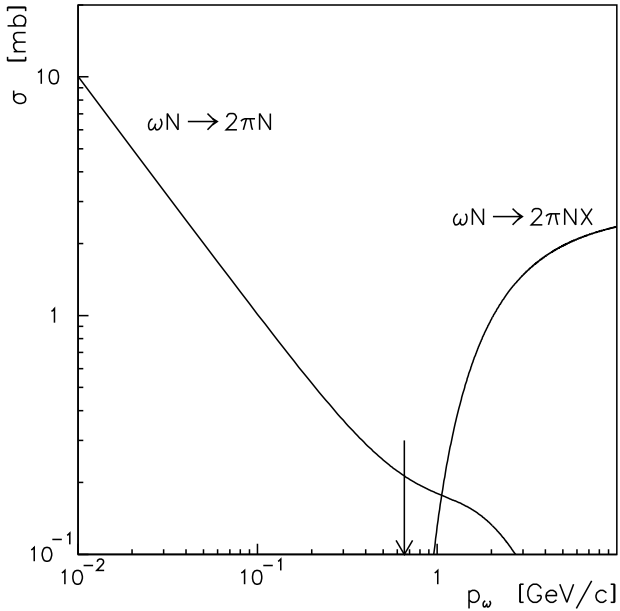


FIG. 7. The exclusive  $\omega N \rightarrow 2\pi N$  and inclusive  $\omega N \rightarrow \pi N X$  cross sections. The arrow indicates the  $\omega N \rightarrow \pi \rho N$  threshold using the  $\rho$  pole mass. The inclusive cross section is calculated for the invariant mass of the  $\pi N$ -system above  $m_\rho + m_N$ .

Now we replace the  $\rho N \rightarrow \pi N$  cross section in Eq. (11) by the total  $\rho N$  cross section taken from Ref. [32] in order to estimate the inclusive  $\omega N \rightarrow \pi N X$  reaction due to  $\rho$ -meson exchange. However, we replace the lower limit of the first integral in Eq. (11) by  $(m_N + m_\rho)^2$ , which allows us to estimate only part of the total cross section. This calculated cross section is shown in Fig. 7 together with the threshold given the bare  $\rho$ -mass (arrow) for momenta above 1 GeV/c.

### E. Elastic $\omega N \rightarrow \omega N$ scattering

We describe elastic  $\omega N$  scattering by the sigma-exchange model shown in terms of the diagram Fig. 1e). The Lagrangian used reads

$$\mathcal{L}_{\sigma NN} = g_{\sigma NN} \bar{N} N \cdot \sigma, \quad (14)$$

$$\mathcal{L}_{\omega\sigma\omega} = g_{\omega\sigma\omega} (\partial^\alpha \omega^\beta \partial_\alpha \omega_\beta - \partial^\alpha \omega^\beta \partial_\beta \omega_\alpha) \sigma, \quad (15)$$

with the scalar coupling constant  $g_{\sigma NN}=10.54$  and monopole form factors with cut-off parameter  $\Lambda=2 \text{ GeV}$  at the  $\sigma NN$  vertex [33].

An upper limit for the  $\omega\sigma\omega$  coupling can be obtained from the  $\omega \rightarrow 2\pi^0\gamma$  partial width assuming that this decay entirely proceeds through the  $\omega \rightarrow \sigma\omega$  process followed by the  $\omega \rightarrow \gamma$  transition due to the vector dominance model and the  $\sigma \rightarrow 2\pi^0$  decay. Starting from the Lagrangian (15) and integrating over the  $\sigma$  spectral function Post [34] obtained  $g_{\omega\sigma\omega}=5.7$  taking into account the most recent data [35] on the  $\omega \rightarrow 2\pi^0\gamma$  decay rate. A coupling  $g_{\omega\sigma\omega}=0.5$  was estimated in Refs. [36,37] from the  $\omega \rightarrow 2\pi^0\gamma$  decay [38] using, however, a different Lagrangian for the  $\omega\sigma\omega$  interaction and replacing the  $\sigma$ -meson spectral function by a  $\delta$ -distribution.

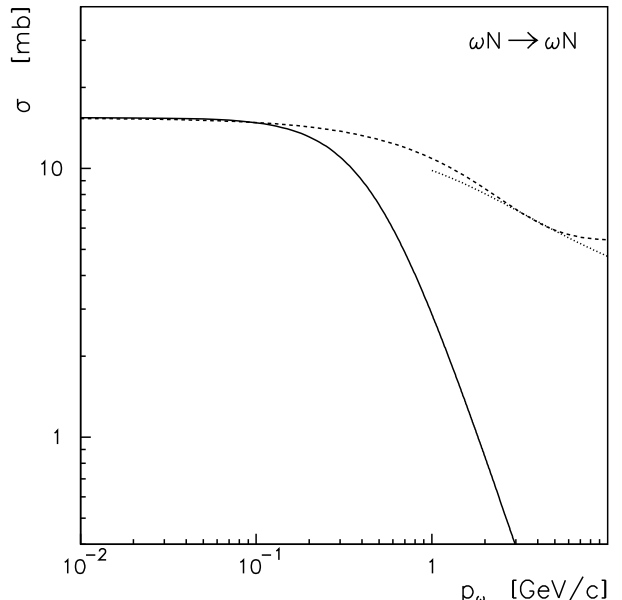


FIG. 8. The  $\omega N \rightarrow \omega N$  elastic cross section. The solid line indicates the calculation within the  $\sigma$ -exchange model for  $g_{\omega\sigma\omega}=1.76$ ; the dotted line is the high energy limit (17), while the dashed line shows our interpolation (18).

On the other hand, as proposed by Singer [39], the  $\omega \rightarrow 2\pi\gamma$  decay may proceed also through the two-step process  $\omega \rightarrow \rho\pi$  followed by the  $\rho \rightarrow \pi\gamma$  transition; the data on the partial  $\omega \rightarrow 2\pi^0\gamma$  width indeed can be entirely described by the latter process. A more sophisticated analysis has been performed by Fajfer and Oakes [40], who consider a three-step process  $\omega \rightarrow \rho\pi$  followed by  $\rho \rightarrow \pi\omega$  and as a last step the  $\omega \rightarrow \gamma$  transition. They predict [40] a branching ratio for the  $\omega \rightarrow 2\pi^0\gamma$  decay of  $8.21 \times 10^{-5}$ , which is compatible to  $(7.2 \pm 2.5) \times 10^{-5}$  as quoted recently by the PDG [35].

We point out that there are no reliable constraints for the  $\omega\sigma\omega$  coupling constant and in the following calculations adopt  $g_{\omega\sigma\omega}=1.76$  keeping it essentially as a free parameter of the model. Furthermore, we use a monopole form factor with cut-off parameter  $\Lambda=2.0 \text{ GeV}$  for the  $\omega\sigma\omega$  vertex. With the latter value for  $g_{\omega\sigma\omega}$  the resulting elastic and inelastic contributions to the  $\omega N$  cross section will be quite moderate and thus serve

as lower limits for the reaction cross sections of interest.

The elastic  $\omega N \rightarrow \omega N$  cross section then can be calculated as

$$\frac{d\sigma}{dt} = \frac{g_{\sigma NN}^2 g_{\omega \sigma \omega}^2}{16\pi m_\omega^2 \lambda(s, m_\omega^2, m_N^2)} (4m_N^2 - t) \frac{F_{\omega \sigma \omega}^2 F_{\sigma NN}^2}{(t - m_\sigma^2)^2} \left( m_\omega^4 - \frac{m_\omega^2 t}{3} + \frac{t^2}{12} \right) \quad (16)$$

with  $m_\sigma = 550$  MeV. The result of this model is shown by the solid line in Fig. 8 and indicates a maximum of  $\approx 15$  mb at low relative momentum but levels off very fast for high momenta.

The high energy limit for the  $\omega N \rightarrow \omega N$  elastic cross section can be taken in the Quark Model [41,42] as

$$\sigma_{\omega N \rightarrow \omega N}(s) = \frac{1}{2} [\sigma_{\pi^+ N \rightarrow \pi^+ N}(s) + \sigma_{\pi^- N \rightarrow \pi^- N}(s)], \quad (17)$$

which is shown in Fig. 8 by the dotted line above momenta of 1 GeV/c. We add that in Eq. (17) the elastic  $\pi^\pm N$  cross section is taken from Ref. [43] and the identity (17) is used at the same invariant energy for the  $\omega N$ - and  $\pi N$ -interaction.

For our following applications to heavy-ion transport simulations we interpolate the  $\omega N$  elastic cross section within the range from 10 MeV/c up to 10 GeV/c as

$$\sigma_{el} = 5.4 + 10 \exp(-0.6p_\omega) \text{ [mb]}, \quad (18)$$

where  $p_\omega$  denotes the laboratory momentum of the  $\omega$ -meson in GeV/c. The parameterization (18) is shown additionally by the dashed line in Fig. 8.

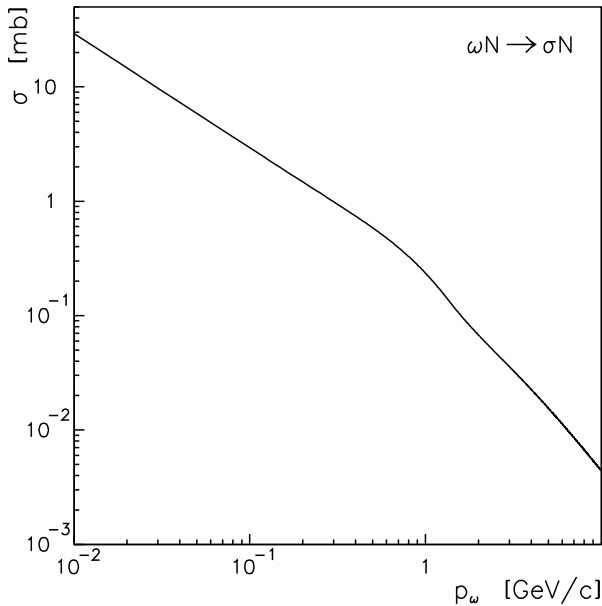


FIG. 9. The  $\omega N \rightarrow \sigma N$  cross section within the  $\omega$ -exchange model for  $g_{\omega \sigma \omega} = 1.76$ .

### F. The channel $\omega N \rightarrow \sigma N$

When incorporating the  $\omega \sigma \omega$ -vertex for elastic  $\omega N$  scattering one has to consider this vertex also in the  $\omega N \rightarrow \sigma N$

reaction due to  $\omega$ -meson exchange as shown in Fig. 1f). The differential cross section for this process is given by

$$\frac{d\sigma}{dt} = \frac{g_{\omega NN}^2 g_{\omega \sigma \omega}^2}{96\pi m_\omega^2} \frac{2t + 4m_N^2}{\lambda(s, m_\omega^2, m_N^2)} \frac{F_{\omega \sigma \omega}^2 F_{\omega NN}^2}{(t - m_\omega^2)^2} [(t - m_\omega^2 - m_\sigma^2)^2 - 4m_\omega^2 m_\sigma^2]. \quad (19)$$

We introduce a monopole form factor at the  $\omega NN$  vertex with the cut-off  $\Lambda = 1.5$  GeV [33]. The parameters for the  $\omega \sigma \omega$  vertex are the same as for the  $\omega N \rightarrow \omega N$  calculations. This results in the  $\omega N \rightarrow \sigma N$  cross section shown in Fig. 9, which also gives up to 30 mb for low  $\omega$  momenta.

### G. The total $\omega N$ cross section

We finally incoherently sum the partial cross sections - calculated for the different  $\omega N$  reaction channels - and show the result in terms of the solid line in Fig. 10.

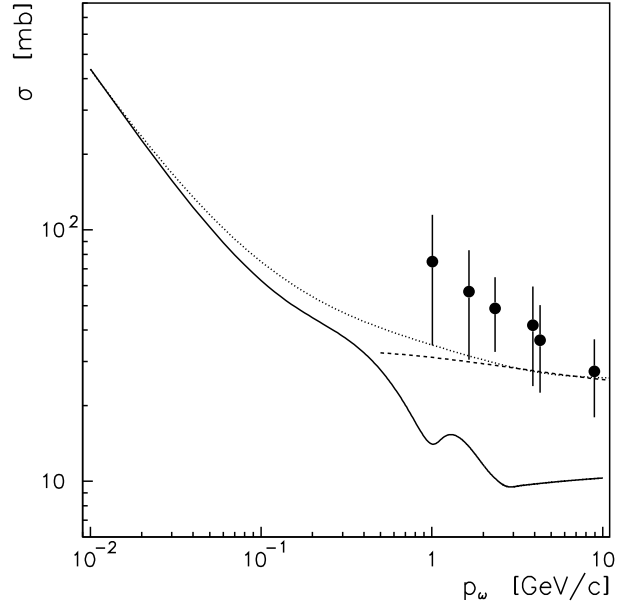


FIG. 10. The total  $\omega N$  cross section as a function of the  $\omega$ -meson momentum in the laboratory system. The solid line shows our result as an incoherent sum of the calculated partial cross sections. The full circles show the results obtained within the VDM from the data on forward  $\omega$ -photoproduction. The dashed line illustrates the estimation from the Quark Model while the dotted line is our parameterization.

In this summation we have taken the cross section for the inclusive  $\omega N \rightarrow \rho N X$  reaction instead of the exclusive  $\omega N \rightarrow \rho \pi N$  reaction. Again at high momenta our result can be compared with the estimate from the Quark Model [41,42] obtained with Eq. (17) by replacing the elastic  $\pi N$  cross section with the total cross section. This result is shown by the dashed line in Fig. 10 and matches with our calculations in the OBE model at momenta of 0.5 GeV/c.

Furthermore, at high momenta the  $\omega N$  total cross section can be estimated within the Vector Dominance Model, where the total  $\omega N$  cross section can be related to the forward  $\gamma N \rightarrow \omega N$  differential cross section as [44]

$$\sigma_{\omega N}^2(s) = \frac{\gamma_\omega^2}{4\pi} \frac{64\pi}{\alpha} \frac{1}{1+\alpha_\omega^2} \left( \frac{q_\gamma}{q_\omega} \right)^2 \frac{d\sigma_{\gamma p \rightarrow \omega p}(s)}{dt} \Big|_{t=0}, \quad (20)$$

where  $q_\gamma$  and  $q_\omega$  are the photon and  $\omega$ -meson momenta in the  $\gamma N$  and  $\omega N$  center-of-mass systems at the same invariant collision energy  $\sqrt{s}$ . In Eq. (20)  $\alpha_\omega$  denotes the ratio of the real to imaginary part of the  $\omega N$  forward scattering amplitude [44], while  $g_\omega$  is the  $\gamma\omega$  coupling constant. We neglect  $\alpha_\omega$  and take  $g_\omega^2/4\pi=4.9$  from Ref. [45]. The full circles (with error bars) in Fig. 10 show the total  $\omega N$  cross section obtained from the experimental data on forward  $\omega$ -meson photoproduction [45,46].

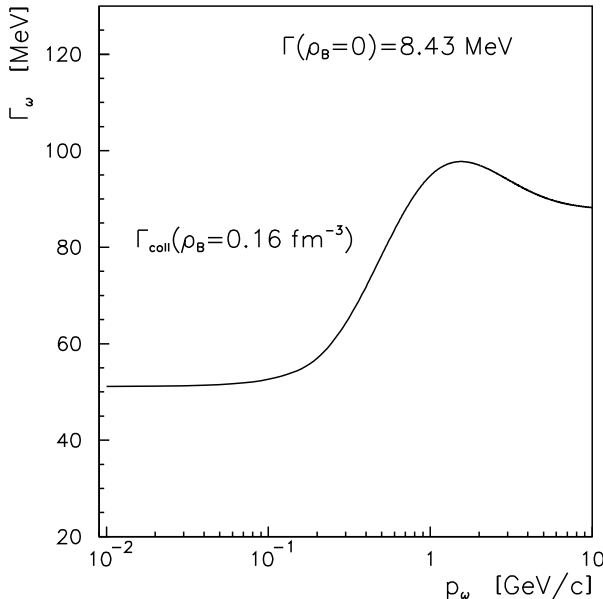


FIG. 11. The in-medium  $\omega$ -meson width due to collisional broadening as a function of the laboratory  $\omega$ -meson momentum.

For the following transport calculations the total inelastic  $\omega N$  cross section is separately fitted and interpolated as

$$\sigma_{inel} = 20 + \frac{4.0}{p_\omega} [\text{mb}], \quad (21)$$

where the laboratory  $\omega$ -meson momentum  $p_\omega$  is given in  $\text{GeV}/c$ . The parameterization for the total  $\omega N$  cross section then is given as a sum of the elastic (18) and inelastic (21) cross section as shown by the dotted line in Fig. 10. Especially the inelastic  $\omega N$  cross section is found to be quite large at low momenta and implies substantial final state interactions of the  $\omega$ -meson in the medium.

In line with these final state interactions the  $\omega$ -meson will change its spectral function in the medium and (in first order) will acquire a larger width due to collisional broadening at baryon density  $\rho_B$ ,

$$\Gamma_{coll}(p_\omega) = \frac{4}{(2\pi)^3} \int d^3 p v_{\omega N} \sigma_{\omega N}(\sqrt{s}) \Theta(p_F - |\mathbf{p}|), \quad (22)$$

with  $v_{\omega N}$  denoting the relative velocity between the  $\omega$ -meson and the nucleon;  $p_F$  is the nuclear Fermi momentum and  $\sqrt{s}$  the invariant energy of the  $\omega N$  system.

The result for  $\Gamma_{coll}$  at density  $\rho_0$  ( $p_F \approx 0.26 \text{ GeV}/c$ ) is shown in Fig. 11 by the solid line as a function of the  $\omega$ -meson momentum relative to the nuclear medium and is about 50 MeV at low  $\omega$  momenta, but increases to 100 MeV above  $p_\omega \approx 1 \text{ GeV}/c$ . Our result is substantially larger at  $p_\omega \approx 0$  than the estimate of 20 MeV in Ref. [16] and slightly larger than the result of Klingl et al. [14] due to the additional channels taken into account in our computations. Nevertheless, the collisional width for  $\omega$ -mesons produced at rest in nuclei is still small compared to its mass.

### III. $\omega$ -PRODUCTION IN HEAVY-ION COLLISIONS

The production of  $\omega$ -mesons from heavy-ion collisions has been calculated previously within the HSD transport approach [47] and is described e.g. in more detail in Ref. [4].

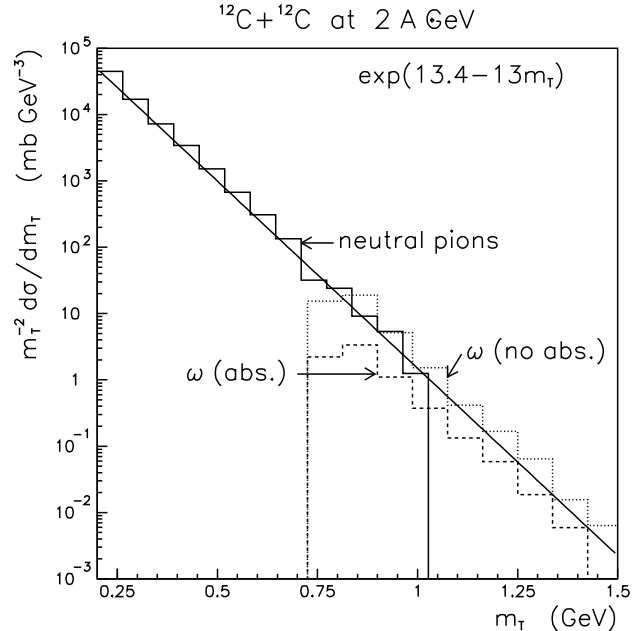


FIG. 12. The inclusive transverse mass spectra for  $\pi^0$  (solid histogram) and  $\omega$ -mesons (divided by a factor of 3 due to the  $\omega$  polarizations) from  $C+C$  collisions at  $2 \text{ A}\cdot\text{GeV}$ . The dashed histogram shows the calculations with all  $\omega N$  interactions while the dotted histogram is obtained without  $\omega$  absorption. The thick solid line indicates the  $m_T$ -scaling.

In these transport simulations the  $\omega$ -absorption as well as elastic scattering in the nuclear environment are explicitly included as well as (optional) a reduction of the  $\omega$  pole mass at finite baryon density. In the present study we concentrate on the impact of the  $\omega N$  final state interactions with nucleons

especially with respect to a global  $m_T$ -scaling suggested by Bratkovskaya et al. [47] for meson production from heavy-ion collisions at SIS energies. The latter scaling was found to be well in line with the spectra for  $\pi^0$  and  $\eta$  mesons as measured by the TAPS Collaboration [48,49].

Employing the elastic and inelastic  $\omega N$  cross sections from Section 2 we have performed calculations without  $\omega$ -potentials in the medium for the systems  $^{12}C+^{12}C$ ,  $^{40}Ca+^{40}Ca$  at 2 A GeV and  $^{58}Ni+^{58}Ni$  at 1.9 A·GeV, which are studied experimentally by the TAPS Collaboration also for  $\omega$ -meson production via the Dalitz decay  $\omega \rightarrow \pi^0 \gamma$ .

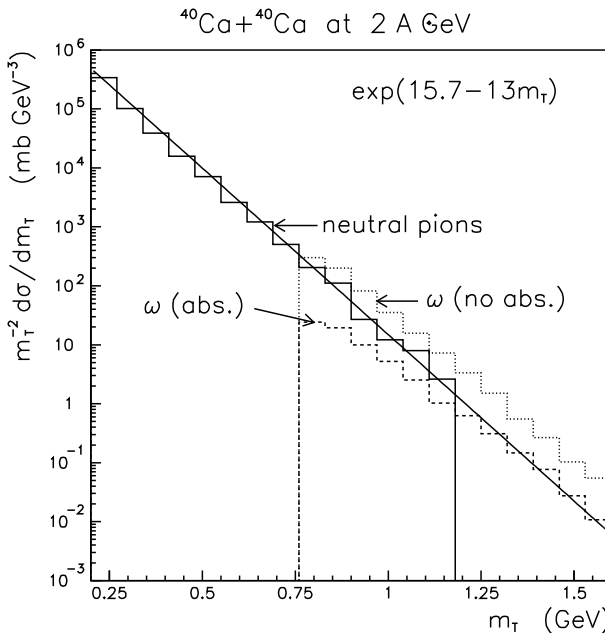


FIG. 13. The inclusive transverse mass spectra for  $\pi^0$  (solid histogram) and  $\omega$ -mesons (divided by the number of polarizations) from  $Ca+Ca$  collisions at 2 A·GeV. The dashed histogram shows the calculations with all  $\omega N$  interactions while the dotted histogram is obtained without  $\omega$  absorption. The thick solid line indicates the  $m_T$ -scaling.

Figs. 12,13,14 show the calculated inclusive transverse mass spectra for  $\pi^0$  and  $\omega$ -mesons with the transverse mass defined as  $m_T = \sqrt{p_T^2 + m^2}$ , where  $p_T$  is the transverse momentum and  $m$  stands for the mass of the meson. The solid histograms in Figs. 12,13,14 show the  $\pi^0$ -meson spectra while the straight solid lines indicate the scaling

$$\frac{1}{m_T^2} \frac{d\sigma}{dm_T} = A \exp(-Bm_T) \quad (23)$$

with parameters  $A$  and  $B$  given in Table I.

Indeed the neutral pions follow the scaling within the statistical accuracy. The transverse mass distributions for the  $\omega$ -meson, which were divided by a factor of 3 as in Ref. [47] due to the 3 different polarizations of the  $\omega$ -meson, are shown by the dotted histograms when neglecting the  $\omega$ -meson absorption in nuclear matter due to the inelastic  $\omega N$  interactions. In this limit the  $m_T$ -scaling is overestimated especially for

$Ca+Ca$  and  $Ni+Ni$ . The dashed histograms show the calculations accounting for the  $\omega$ -absorption as well as  $\omega N \rightarrow \omega N$  elastic scattering. In all cases the  $m_T$ -scaling relative to neutral pions is underestimated especially for low transverse mass of the  $\omega$ -mesons which results from the large absorption cross section for  $\omega$ -mesons at low relative momenta according to Section 2.

TABLE I. Parameters of the  $m_T$ -scaling approximation (23).

System	$C + C$	$Ca + Ca$	$Ni + Ni$
Energy (A·GeV)	2.0	2.0	1.9
$A$ (b·GeV $^{-3}$ )	660	6583	9821
$B$ (GeV $^{-1}$ )	13	13	13

Fig. 15 shows the nuclear transparency coefficient as a function of the  $\omega$ -meson momentum in the center-of-mass for  $C + C$ ,  $Ca + Ca$  and  $Ni + Ni$  systems. Here the nuclear transparency coefficient is defined as the ratio of the  $\omega$ -mesons detected asymptotically for  $t \rightarrow \infty$  to the total number of the  $\omega$ -mesons produced in elementary pion-baryon and baryon-baryon collisions. The effect is most pronounced for slow  $\omega$ -mesons since the inelastic  $\omega N$  interaction is very strong at low momenta (cf. Fig. 10).

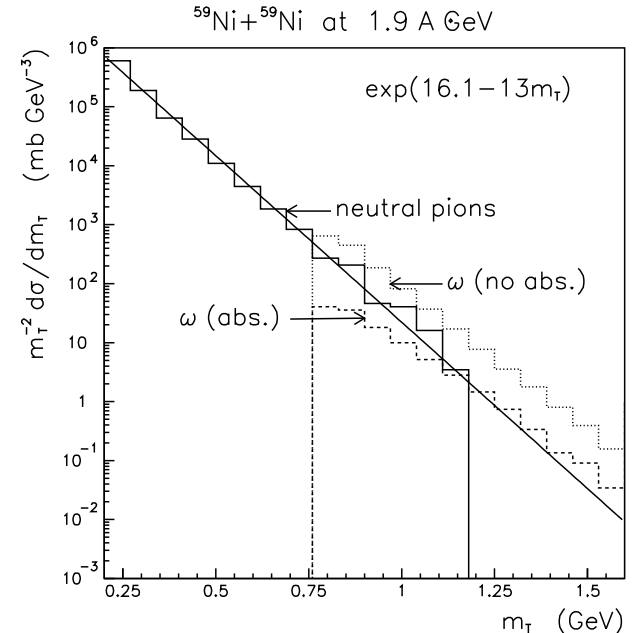


FIG. 14. The inclusive transverse mass spectra for  $\pi^0$  (solid histogram) and  $\omega$ -mesons from  $Ni+Ni$  collisions at 1.9 A·GeV. The dashed histogram shows the calculations with all  $\omega N$  interactions while the dotted histogram is obtained without  $\omega$  absorption. The thick solid line indicates the  $m_T$ -scaling.

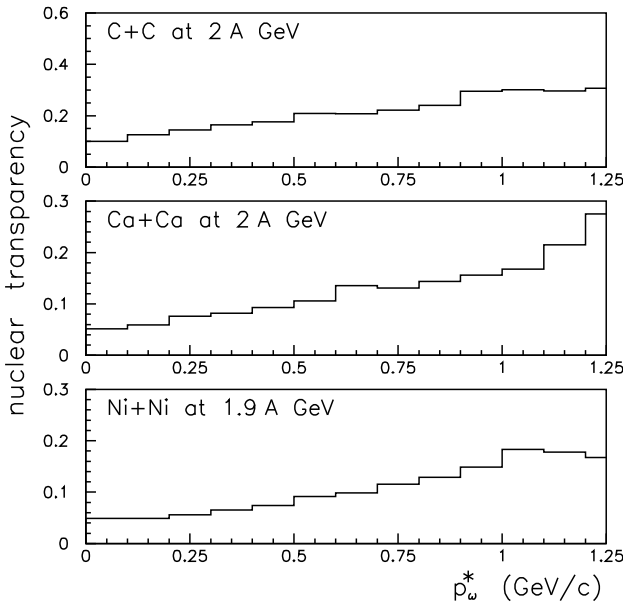


FIG. 15. The nuclear transparency coefficient as a function of the  $\omega$ -momentum in the center-of-mass system for  $C + C$ ,  $Ca + Ca$  and  $Ni + Ni$  collisions at 2.0 and 1.9 A GeV, respectively.

Table II shows the inclusive  $\omega$ -meson production cross section for  $C + C$ ,  $Ca + Ca$  and  $Ni + Ni$  collisions calculated with and without  $\omega N$  final state interactions. Even for the light system  $C + C$  the  $\omega$  production cross section is reduced by a factor  $\simeq 4.5$  due to strong absorption.

TABLE II. Inclusive  $\omega$ -meson production cross section from  $C + C$ ,  $Ca + Ca$  and  $Ni + Ni$  collisions calculated with and without final state interactions of the  $\omega$  mesons.

System	$C + C$	$Ca + Ca$	$Ni + Ni$
Energy (A·GeV)	2.0	2.0	1.9
$\sigma$ (mb) with FSI	1.42	10.56	19.5
$\sigma$ (mb) without FSI	6.52	91.4	206.8

#### IV. SUMMARY

Within the meson exchange model we have calculated different partial cross sections for the  $\omega N$  interaction, i.e.  $\omega N \rightarrow \pi N$ ,  $\omega N \rightarrow \rho N$ ,  $\omega N \rightarrow \omega N$ ,  $\omega N \rightarrow \rho \pi N$ ,  $\omega N \rightarrow \rho N X$ ,  $\omega N \rightarrow 2\pi N$ ,  $\omega N \rightarrow 2\pi N X$  and  $\omega N \rightarrow \sigma N$  reaction channels. The free parameters of the model were fixed by the available experimental data on the  $\pi N \rightarrow \omega N$  reaction [23–25] or adopted from the study on vector meson photoproduction [20] except for the  $\omega \sigma \omega$ -vertex, where we have adopted a conservative low coupling constant.

At high energies, i.e.  $\omega$  momenta above a few GeV/c, the total cross section approaches a conventional hadronic cross section of  $\simeq 25$  mb according to the prediction from the Quark Model as well as the estimate from the Vector Dominance model. The total cross section at low  $\omega$  momenta according to the

OBE model sums up to a few hundred mb which indicates a sizeable rescattering and reabsorption of the  $\omega$ -meson in the nuclear medium. The collisional broadening of the  $\omega$ -meson at nuclear matter density  $\rho_0$  amounts to about 50 MeV at rest, but increases with momentum up to 100 MeV. Thus the  $\omega$  spectral function at  $\rho_0$  is dominated by the hadronic couplings in the medium.

Furthermore, we have investigated the impact of the  $\omega N$  final state interactions on  $\omega$ -production in heavy-ion collisions around 2 A·GeV. It is found that due to strong absorption the total  $\omega$ -meson production cross section from  $C + C$  collisions at SIS energies is reduced by a factor of  $\simeq 4.5$  and by a factor of  $\simeq 10$  for  $Ni + Ni$  collisions. Furthermore, we find a significant deviation from the  $m_T$ -scaling behaviour predicted in Ref. [47] for  $\omega$ -meson production in heavy-ion collisions due to the strong final state interactions for slow  $\omega$ -mesons. These  $m_T$  distributions might be controlled by the TAPS Collaboration in near future.

#### ACKNOWLEDGMENTS

The authors like to thank V. Metag and H. Löchner for valuable discussions throughout this study. This work was supported by BMBF, Forschungszentrum Jülich and the Russia Foundation for the fundamental Research

---

- [1] J.W. Harris and B. Müller, Ann. Rev. Nucl. Part. Sci. **bf 46**, 71 (1996).
- [2] C.M. Ko and G.Q. Li, J. Phys. G **bf 22**, 1673 (1996).
- [3] G.E. Brown and M. Rho, Phys. Rev. Lett. **bf 66**, 2720 (1991).
- [4] W. Cassing and E.L. Bratkovskaya, Phys. Rep. (1998) in print.
- [5] S. Leupold, W. Peters and U. Mosel, Nucl. Phys. **A628**, 311 (1998).
- [6] R. Rapp, G. Chanfray and J. Wambach, Phys. Rev. Lett. **76**, 368 (1996); Nucl. Phys. **A617**, 472 (1997).
- [7] W. Peters, M. Post, H. Lenske, S. Leupold and U. Mosel, Nucl. Phys. **A632**, 109 (1998).
- [8] B. Friman and H.J. Pirner, Nucl. Phys. **A617**, 496 (1997).
- [9] W. Schön, H. Bokemeyer, W. Koenig and V. Metag, Acta Phys. Pol. B **27**, 2959 (1996).
- [10] W. Cassing, Ye.S. Golubeva, A.S. Iljinov and L.A. Kondratyuk, Phys. Lett. B **396**, 26 (1997).
- [11] Ye. S. Golubeva, L.A. Kondratyuk and W. Cassing, Nucl. Phys. **A625**, 832 (1997).
- [12] F. Klingl, N. Kaiser and W. Weise, Nucl. Phys. **A624**, 527 (1997).
- [13] F. Klingl and W. Weise, hep-ph/9802211.
- [14] F. Klingl, T. Waas and W. Weise, hep-ph/9810312.
- [15] B. Friman, nucl-th/9801053.
- [16] B. Friman, nucl-th/9808071, to be publ. in Acta Phys. Pol. B

- [17] W. Ehehalt and W. Cassing, Nucl. Phys. **A602**, 449 (1996).
- [18] M. Gell-Mann, D. Sharp and W.G. Wagner, Phys. Rev. Lett. **8**, 261 (1962).
- [19] N.M. Kroll, T.D. Lee and B. Zumino, Phys. Rev. **157**, 1376 (1967).
- [20] B. Friman and M. Soyeur, Nucl. Phys. **A600**, 475 (1996).
- [21] F. Klingl, N. Kaiser and W. Weise, Z. Phys. A **356**, 193 (1996); F. Klingl, private communication.
- [22] A. Sibirtsev, W. Cassing, G.I. Lykasov and M.V. Rzjanin, Nucl. Phys. **A632**, 131 (1998).
- [23] R. J. Miller, S. Lichtman and R.B. Willmann, Phys. Rev. **178**, 2061 (1969).
- [24] L.E. Holloway et al., Phys. Rev. D **8**, 2814 (1973).
- [25] Landolt-Börnstein, New Series, ed. H. Schopper, I/12 (1988).
- [26] J.J. De Swart, M.C.M. Rentmeester and R.G.E. Timmermans, nucl-th/9802084.
- [27] A. Sibirtsev, K. Tsushima and A.W. Thomas, Phys. Lett. B **421**, 59 (1998).
- [28] V.B. Berestetsky and I.Ya. Pomeranchuk, Nucl. Phys. **22**, 629 (1961).
- [29] E. Ferrari and F. Selleri, Suppl. Nuovo Cim. **24**, 451 (1962).
- [30] A. Engel et al., Nucl. Phys. **A603**, 387 (1996).
- [31] A. Sibirtsev, W. Cassing and U. Mosel, Z. Phys. **A358**, 357 (1997).
- [32] L. A. Kondratyuk, A. Sibirtsev, W. Cassing, Ye. S. Golubeva, and M. Effenberger, Phys. Rev. C **58**, 1078 (1998).
- [33] R. Machleid, K. Holinde and Ch. Elster, Phys. Rep. **149**, 1 (1987).
- [34] M. Post, private communication.
- [35] Particle Data Group, Eur. Phys. J. A **3**, 1 (1998).
- [36] K. Nakayama, A. Szczurek, C. Hanhart, J. Haidenbauer, and J. Speth, Phys. Rev. C **57**, 1580 (1998).
- [37] C. Hanhart, private communication.
- [38] Particle Data Group, Phys. Rev. D **54**, 1 (1996).
- [39] P. Singer, Phys. Rev. **128**, 2789 (1962); **130**, 2441 (1963); **161**, 1694 (1967).
- [40] S. Fajfer and R.J. Oakes, Phys. Rev. D **42**, 2392 (1990).
- [41] H.J. Lipkin, Phys. Rev. Lett. **16**, 1015 (1966).
- [42] K. Kajantie and J.S. Trefil, Phys. Lett. B **24**, 106 (1967).
- [43] Particle Data Group, Phys. Rev. D **50**, 1173 (1994).
- [44] T.H. Bauer, R.D. Spital, D.R. Yennie and F.M. Pipkin, Rev. Mod. Phys. **50**, 261 (1978).
- [45] J. Ballam et al., Phys. Rev. D **7**, 3150 (1973).
- [46] Landolt-Börnstein, New Series, ed. H. Schopper, **8** (1973).
- [47] E.L. Bratkovskaya, W. Cassing and U. Mosel, Phys. Lett. B **424**, 244 (1998).
- [48] R. Averbeck et al., Z. Phys. A **359**, 65 (1997).
- [49] M. Appenheimer et al., GSI Annual Report 1996, 58.